Supplemental Materials for

Teamwork in the viscous oceanic microscale

Eva Kanso, Rubens M. Lopes, J. Rudi Strickler, John O. Dabiri, and John H. Costello

April 15, 2021

Diatom model

Spherical diatom approximation. Diatoms are cylindrical in shape. A cylinder might be expected to sink differently than a sphere in the viscous Stokes regime. However, a spherical model was shown to best fit diatom sinking rates and did not significantly differ from that of a cylindrical model [1]. The authors in [1] suggest that other terms, such as relative frustule thickness - which can vary substantially between similarly shaped cells - affects sinking rate more than the comparatively small difference between spherical and circular shapes in sinking rates. Since the relative shape effects for important variables of this study, such as sinking, were negligible, we believed that the spherical assumption used in the model is a useful and reasonable approximation for diatom cells. Hereafter, we model the diatom as a sphere of radius R.

The spherical diatom model has also been used extensively to study the concentration boundary layer around suspended and sinking diatoms [2], hence reinforcing the feasibility of the spherical diatom assumption.

Pure diffusion

Diffusion-only nutrient uptake. Consider the case in which only molecular diffusion in the suspending fluid governs transport (uptake or rejection) of a chemical species whose concentration is $C(r)$, where r is the radial distance from the center of the diatom, which we approximate to be a sphere of radius R. When more than even a few percent of the diatom surface is covered by an array of absorbers (or emitters), the diffusion-limited rate is well approximated by that of a surface uniformly covered with absorbers (or emitters); see [3]. Here, we focus on nutrient acquisition (absorbers only), implying zero concentration at the diatom surface. At large distance r from the diatom, the concentration is at ambient levels. By Fick's law, a gradient in concentration yields a flux. The nutrient uptake rate is the area integral of the flux over the diatom surface $I = -\oint \mathbf{n} \cdot D\nabla C \mathrm{d}S$, where D is the diffusion constant, $\mathbf{n}$ is the unit normal, and $\mathrm{d}S = 2\pi R^2 \sin\theta \mathrm{d}\theta$ is the element of surface area of the sphere (assuming axisymmetry in the ϕ-coordinate). This sign convention is such that the concentration flux is positive if the sphere takes up nutrients. If C_∞ is the ambient concentration level far from the diatom, then the steady-state concentration is $C(r) = C_\infty(1 - R/r)$, which we obtain by solving the diffusion equation $D\Delta C = 0$ in the unbounded domain outside a sphere. At steady state, the diffusion boundary layer characterized by nutrient depletion region around the diatom extends up to nine body lengths from the diatom surface before the nutrient concentration reaches 90% of ambient levels, creating formidable disadvantages for nutrient acquisition [2]. The steady state inward current due to molecular diffusion $I_{\text{diffusion}} = 4\pi RDC_\infty$ is linear in the diatom size R.

Size limitations. The nutrient diffusion-based flux $I_{\text{diffusion}}$ can be compared with the metabolic requirements of the 'spherical' diatom $I_{\text{metabolic}} = (4\pi R^3/3)\beta$, where β is the time-dependent nutrient demand rate per unit volume [4]. The availability by diffusion can exceed the nutritional requirements at small radii. When metabolic requirements are equal to diffusive nutrient flux $I_{\text{metabolic}} = I_{\text{diffusion}}$, we get a critical diatom radius $R_{\text{cr}} = \sqrt{3DC_\infty/\beta}$. Estimation of the critical diatom size includes several considerations. First, the demand or consumption rate β varies with time and environmental parameters (e.g., light, temperature,

Table S1: **Parameter values** of the environment and **Characteristic scales** of a sinking diatom and a diatom-ciliate system with a single attached ciliate

Parameter	**Symbol**	**Dimensional value**
Fluid density 20^oC	ρ	$1000\ \mathrm{kg \cdot m^{-3}}$
Fluid viscosity 20^oC	η	$10^{-3}\ \mathrm{Pa \cdot s} = 10^{-3}\ \mathrm{kg \cdot m^{-1} \cdot s^{-1}}$
Nutrient diffusivity 20^oC	D	$10^{-9}\ \mathrm{m^2 \cdot s^{-1}}$
Acceleration due to gravity	g	$9.80\ \mathrm{m \cdot s^{-2}}$
Diatom radius	R	$100\ \mu$m
Diatom-water density difference	$\Delta\rho$	10 – $100\mathrm{kg \cdot m^{-3}}$
Diatom sinking velocity from Eq. (1)	U	$200 - 2000\ \mu\mathrm{m \cdot s^{-1}}$
Péclet number	$\mathrm{Pe} = RU/D$	20 – 200
Reynolds number	$\mathrm{Re} = \rho UR/\eta$	0.02 – 0.2
Ciliate height	h	$45\ \mu$m
Ciliated-ring diameter	2δ	$40\ \mu$m
Ciliate-induced flow (diatom-single ciliate)	U	100 – $500\ \mu\mathrm{m \cdot s^{-1}}$
Ciliate force (single ciliate)	$F = \eta U\delta$	2 – 10 pN
Péclet number (diatom-single ciliate)	$\mathrm{Pe} = RU/D$	10 – 50
Reynolds number	$\mathrm{Re} = \rho UR/\eta$	0.01 – 0.05

nutrient availability) during the life cycle of the diatom. Second, there is uncertainty as to which of the key nutrients is limiting. Third, the boundary condition for waste rejection at the diatom surface may affect the nutrient flux. Mindful of these difficulties, we can make rough estimates by considering empirical values for β and C_∞.

To obtain such values, we looked at other microscopic systems of similar size and shape such as the multicellular spherical colonies of *Volvox carteri* considered in [4]. The authors used parameters appropriate for phosphate ($D = 10^{-5}\ \mathrm{cm^2 \cdot s}$, $C_\infty = 6 \times 10^{14}\ \mathrm{cm^{-3}}$, and $\beta = 10^{12}\ \mathrm{cm^{-2} \cdot s^{-1}}$) and oxygen ($D = 2 \times 10^{-5}\ \mathrm{cm^2 \cdot s}$, $C_\infty = 10^{17}\ \mathrm{cm^{-3}}$, and $\beta = 10^{14}\ \mathrm{cm^{-2} \cdot s^{-1}}$) in deriving size estimates for *V. carteri* for which the metabolic requirements scale with the surface area of the spherical colony. Here, the metabolic requirements scale with the volume of the diatom and we have no explicit estimates for β in units of $\mathrm{cm^{-3} \cdot s^{-1}}$. However, progress can be made by assuming a sensible range of values for β, say, $\beta = 10^{14}$–10^{16} in units of $\mathrm{cm^{-3} \cdot} s^{-1}$, which in turn leads to a rough estimate for β/C_∞ between 1 and 0.1 in units of s^{-1}. Considering $\beta/C_\infty = 0.1$, and using $D = 10^{-5}\ \mathrm{cm^2 \cdot s}$ (as in the case of phosphate and dissolved silica), we get that $R_{\mathrm{cr}} \sim \sqrt{3DC_\infty/\beta}$ is approximately equal to $R_{\mathrm{cr}} \approx 175\ \mu$m. For $\beta/C_\infty = 1$, we get $R_{\mathrm{cr}} \approx 50\ \mu$m. This range of R_{cr} is comparable to the range observed in diatoms. Larger diatoms would barely be able to obtain sufficient nutrients by diffusion alone.

Sinking diatom

Sinking diatom. To thin the depletion boundary layer, diatoms sink by regulating their buoyancy [2, 5, 6]. Estimates suggest that the density difference $\Delta\rho$ between the diatom and ambient water can range between $\Delta\rho = 0.01\rho$ and 0.1ρ, where ρ is the water density. To estimate the range of sinking velocities, we use the Stokes' equation for sinking spheres in which the drag force and the submerged weight W are balanced,

$$F_{\mathrm{drag}} = W \quad \Longrightarrow \quad 6\pi\eta R U_{\mathrm{sink}} = (\Delta\rho) g \frac{4}{3}\pi R^3 \quad \Longrightarrow \quad U_{\mathrm{sink}} = \frac{2gR^2\Delta\rho}{9\eta}. \tag{1}$$

Here, η is the fluid viscosity ($10^{-3}\ \mathrm{kg \cdot m^{-1} \cdot s^{-1}}$) and g is the acceleration of gravity ($9.8\ \mathrm{m \cdot s^{-2}}$). For $\Delta\rho = 10\ \mathrm{kg \cdot m^{-3}}$ and $R = 100\ \mu$m, the sinking velocity is $U_{\mathrm{sink}} \approx 220\ \mu\mathrm{m \cdot s^{-1}}$. At the same radius, for $\Delta\rho = 100\ \mathrm{kg \cdot m^{-3}}$, we get $U_{\mathrm{sink}} \approx 2200\ \mu\mathrm{m \cdot s^{-1}}$.

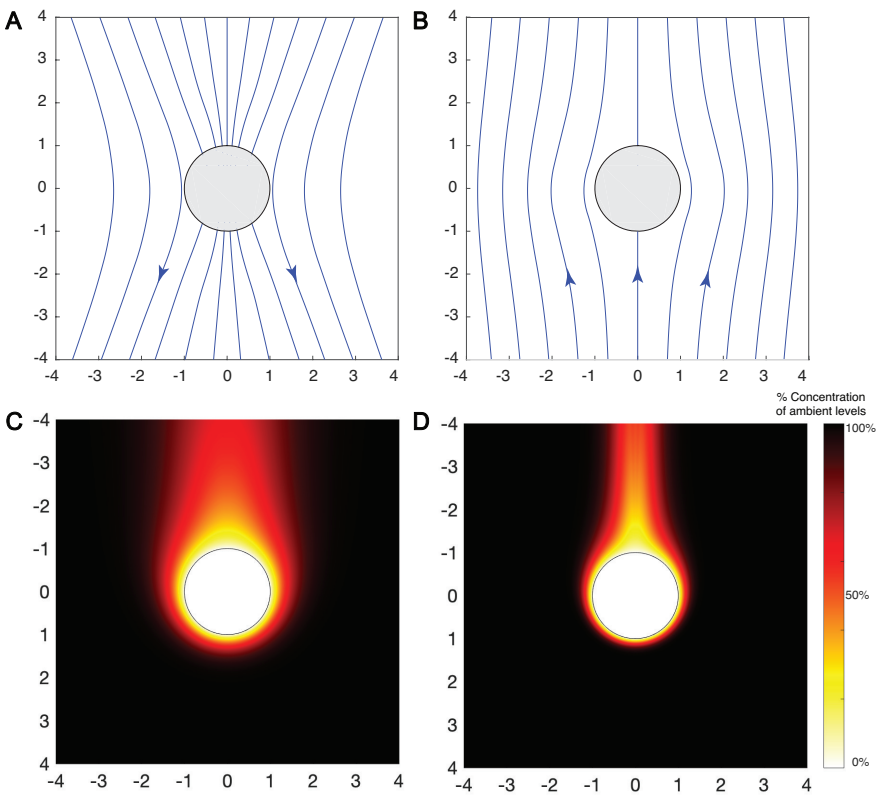

Figure S1: **Sinking diatom:** Streamlines of the velocity field created by a sinking sphere (A) in lab frame and (B) in a frame moving with the sphere. The sphere's radius and sinking velocity are normalized to 1. Concentration field around a sinking sphere at (C) Pe = 10 (Sh = 1.9) and (D) Pe = 100 (Sh = 3.4).

Fluid velocity around a sinking diatom. To find the fluid velocity field $\mathbf{u}$ around a sphere translating at a constant speed $U = U_{\text{sink}}$, we can analytically solve the incompressible Stokes equation

$$\eta \Delta \mathbf{u} - \nabla p = \mathbf{0}, \qquad \nabla \cdot \mathbf{u} = \mathbf{0}, \tag{2}$$

subject to the no-slip boundary conditions at the sphere's surface and proper decay at infinity

$$\mathbf{u}|_{r=R} = U\mathbf{e}_z, \qquad \mathbf{u}|_{r\to\infty} = \mathbf{0}. \tag{3}$$

Here, $\mathbf{e}_z$ is a unit vector pointing vertically downward, in the direction of the acceleration due to gravity, and p is the pressure field. These equations can be solved analytically using spherical coordinates (r, θ, ϕ) in a body-frame attached to the sinking diatom. Considering that the flow is axisymmetric and thus independent of the azimuthal direction ϕ, the velocity components in the frame of the moving sphere are given by [7]

$$u_r = -U(1 - \frac{3R}{2r} + \frac{R^3}{2r^3})\cos\theta, \qquad u_\theta = U(1 - \frac{3R}{4r} - \frac{R^3}{4r^3})\sin\theta. \tag{4}$$

Fig. S1 shows the fluid streamlines around a sinking sphere as seen in a lab frame and in a frame attached to the sinking sphere.

Nutrient concentration around a sinking diatom. How does advection, the transport of solutes by flow around a sinking diatom, modify nutrient uptake? The equation governing the steady-state advection-diffusion of nutrients is given by

$$\mathbf{u} \cdot \nabla C = D\Delta C. \tag{5}$$

Here, $\mathbf{u}(r, \theta)$ is steady-state fluid velocity whose components are given in Eqs. (4), $\mathbf{u}\cdot\nabla C$ is the advective rate of change of the concentration field $C(r, \theta)$, and $D\Delta C$ is the diffusive rate of change. The standard measure

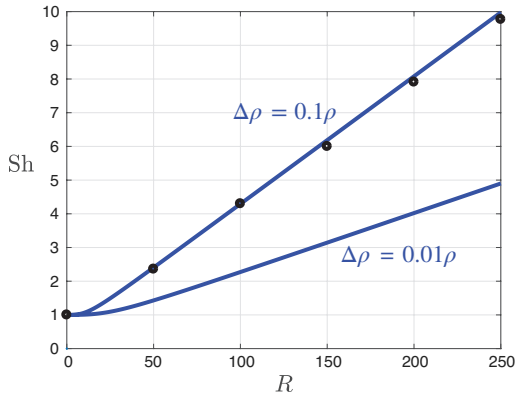

Figure S2: **Sherwood number of sinking diatom:** solid lines correspond to the formula in Eq. (11) based on [8] for $\Delta\rho/\rho$ equal to 0.01 and 0.1 as reported in [2]. Data points shown in '$\circ$' are calculated based on the numerical solution of the advection-diffusion equation in (7). The agreement between the numerics and analytical solution for a range of diatom sizes serves to validate our numerical methods. Here, $\Delta\rho = 10$ kg $\cdot$ m^{-3} for the lower bound and $\Delta\rho = 100$ kg $\cdot$ m^{-3} for the upper bound.

of the competition between advection and diffusion is the (dimensionless) Péclet number $\mathrm{Pe} = RU/D$ which is expressed in terms of a typical flow velocity U (here taken to be the sinking velocity U_{sink} from (1)), the diatom radius R, and the molecular diffusivity D. Indeed, considering R as the length scale and $T_{\mathrm{adv}} = R/U$ as the time scale, the advection-diffusion equation can be rewritten in dimensionless form as follows

$$\mathrm{Pe}\,\mathbf{u}\cdot\nabla C = \Delta C \tag{6}$$

The axisymmetric solution $C(r,\theta)$ to this equation can be obtained either numerically, by direct discretization of the advective terms and the Laplacian operator, or semi-analytically by using an expansion of $C(r,\theta)$ in terms of the Legendre polynomials of $\cos\theta$ [9]. Here, we use a numerical approach as detailed next.

Numerical discretization of the advection-diffusion equation. We rewrite (6) in spherical coordinates, taking into account the axisymmetry of the problem,

$$\mathrm{Pe}\left(u_r\frac{\partial C}{\partial r} + u_\theta\frac{1}{r}\frac{\partial C}{\partial \theta}\right) = \frac{1}{r^2}\frac{\partial}{\partial r}\left(r^2\frac{\partial C}{\partial r}\right) + \frac{1}{r^2\sin\theta}\frac{\partial}{\partial\theta}\left(\sin\theta\frac{\partial C}{\partial\theta}\right). \tag{7}$$

The velocity components u_r and u_θ are given in (4). We set the computational domain such that $r\in[R,10R]$ and $\theta\in[0,\pi]$. We discretize the (r,θ) space in equal increments Δr and $\Delta\theta$ such that $r_i = R + i\Delta r$, with $i = 1,\ldots,N_r$ and $\theta_j = j\Delta\theta$, with $j = 1,\ldots,N_\theta$. For convenience, we use the notation $C_{i,j}$ to denote the concentration $C(r_i,\theta_j)$. We use a second-order central difference scheme to discretize the derivative terms in (7). Specifically, we use

$$\frac{\partial C}{\partial r} = \frac{C_{i+1,j} - C_{i-1,j}}{2\Delta r}, \qquad \frac{\partial C}{\partial\theta} = \frac{C_{i,j+1} - C_{i,j-1}}{2\Delta\theta}, \tag{8}$$

and

$$\frac{\partial^2 C}{\partial r^2} = \frac{C_{i+1,j} - 2C_{i,j} + C_{i-1,j}}{(\Delta r)^2}, \qquad \frac{\partial^2 C}{\partial\theta^2} = \frac{C_{i,j+1} - 2C_{i,j} + C_{i,j-1}}{(\Delta\theta)^2}. \tag{9}$$

We impose Dirichelet boundary conditions at $r = R$ and $r = 10R$ and we use symmetry of solution at $\theta = 0$ and $\theta = \pi$ to obtain boundary conditions at these end points.

The concentration fields around the sinking diatom at two Péclet numbers Pe = 10 and 100 are shown in Fig. S1. The Sherwood number, defined below as the ratio of total nutrient uptake (advective + diffusive) to diffusive nutrient uptake, for diatoms sinking at Pe = 10 is Sh = 1.9, and at Pe = 100, Sh = 3.4. That is to say, the diatom gains twice to four times as much benefit in comparison to pure diffusion when sinking. To benchmark our numerical method, we compare the Sherwood number obtained numerically to a known analytical solution for the sinking diatom [8, 2]. The comparison is shown in Fig. S2 and shows good agreement between the numerics and the analytical solution for a range of diatom sizes.

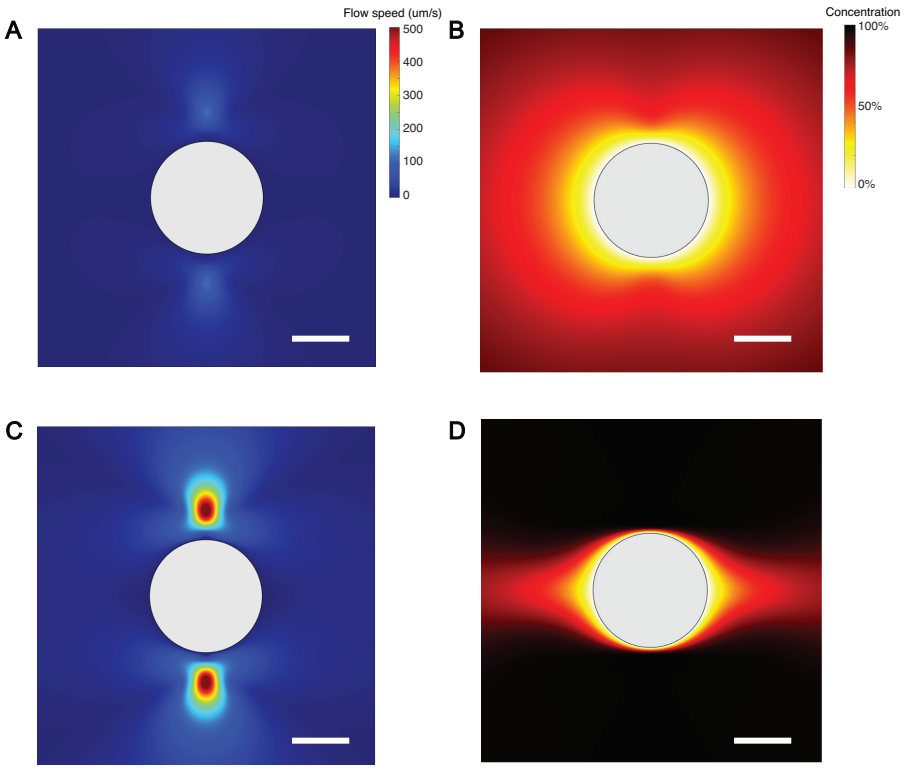

Figure S3: **Diatom-ciliate association:** (A) Flow speed created by a diagonally-opposed pair of ciliates modeled as Stokeslets of dimensionless strength $\tilde{F} = 5$ that are radially-directed towards the sphere's center. (B) Concentration field for Pe = 10 corresponding to an advective time scale $T_{\text{adv}} = 1$ s and a diffusive time scale $T_{\text{diff}} = 10$ s (see Table S2). (C) Flow speed for a pair of Stokeslets of dimensionless strength $\tilde{F} = 25$. (D) Concentration field for Pe = 100 corresponding to an advective time scale $T_{\text{adv}} = 0.2$ s and a diffusive time scale $T_{\text{diff}} = 20$ s (see Table S2). The Sherwood number in (B) and (D) is equal to Sh = 1.13 and 3.89, respectively (see Table S3). Scale bars represent 100 microns in length.

Diatom-ciliate system

Diatom-ciliate flows. Experimental measurements of the typical fluid velocity created by the *Pseudovorticella coscinodisci* when attached to the surface of the diatom *Coscinodiscus wailesii* show that the typical velocity U is of the order of $100 - 500$ $\mu\text{m}\cdot\text{s}^{-1}$. Considering a diatom of radius $R = 100$ μm and a diffusivity coefficient $D = 10^{-9}$ $\text{m}^2\cdot\text{s}^{-1}$, Pe can range from 10 to 50 for a single ciliate. Diatoms are often found in association with multiple ciliates, indicating that this is a conservative estimate of Pe and that advection of nutrient by the ciliate induced currents is dominant.

Ciliate applied force. Because we seek to understand the effect of advective transport on nutrient uptake, we require a model of the flow field created by the ciliate. It is impractical to calculate the detailed flow generated by the array of cilia around the ciliated ring of the *Pseudovorticella coscinodisci*. Instead, we employ a simple model in which the details of the cilia length, beating frequency, and waveform are subsumed into a single averaged parameter, the force F that the ciliate exerts on the fluid. Modeling sessile ciliates as point forces (also referred to as *Stokeslet*) is a common practice in studying ciliates attached to flat walls [10, 11]. Here, we extend these models to ciliates attached to diatoms. Namely, we consider forces applied to the fluid domain outside a spherical surface.

Dimensional analysis shows that the characteristic magnitude of the ciliate force scales as $F \sim \eta U \delta$. For $R = 20$ μm and $U = 500$ $\mu\text{m}\cdot\text{s}^{-1}$, we get $F = 10$ pN (see Table S1), consistent with existing estimates [11].

Sphere-force model. We use the method of images to find the fluid velocity generated by a Stokeslet force outside the sphere and satisfying the zero-flow boundary condition at the sphere's surface; see e.g., [12] for a comprehensive overview of these techniques. Specifically, we use the regularized Stokeslet solution

Table S2: **Characteristic parameters. Dimensional:** we list the characteristic length and time scales in dimensional units obtained from experimental observations (see table S1). **Dimensionless:** we list the non-dimensional parameters used in our computational study. The Stokeslet location is based on relative ciliate-diatom length scale $\tilde{h} = h/R$ and the Stokeslet regularization parameter $\tilde{\delta} = \delta/R$ is based on the radius of the ciliated crown relative to the diatom length scale (see Fig S5 and Table S7). To compute the fluid velocity in the model, we provide as input the strength $\tilde{F}$ of the regularized Stokeslet, the Stokeslet location $\tilde{h} = h/R$, the Stokeslet regularization parameter $\tilde{\delta} = \delta/R$; we compute as output the fluid velocity field and corresponding dimensionless speed $\tilde{U}$. We calibrate the value of $\tilde{F}$ to correspond to a maximal speed U in the range of 100–500 $\mu\text{m} \cdot \text{s}^{-1}$ when the ciliate is attached to a diatom of radius $R = 100$ μm. To estimate the Péclet number, we consider a characteristic chemical diffusivity coefficient $D = 5 \cdot 10^{-10}\text{m}^2 \cdot \text{s}^{-1}$ to obtain an upper estimate and $D = 10^{-9}\text{m}^2 \cdot \text{s}^{-1}$ for the lower estimate.

Dimensional	R	h	F	U	$T_{\text{adv}} = \frac{R}{U}$	$T_{\text{diff}} = \frac{R^2}{D}$	$\text{Pe} = \frac{T_{\text{diff}}}{T_{\text{adv}}}$
	100	50	$\sim \eta U \delta$	500	0.2	20	100
(units)	(μm)	(μm)	(pN)	($\mu\text{m}\cdot\text{s}^{-1}$)	(s)	(s)	–
Dimensionless	$\tilde{R} = \frac{R}{R}$	$\tilde{h} = \frac{h}{R}$	$\tilde{F}$	$\tilde{U}$	$\frac{\tilde{R}}{\tilde{U}}$	$\frac{\tilde{R}}{\tilde{U}}\text{Pe}$	Pe
	1	0.5	25	≈ 5	0.2	20	100
Dimensional	R	h	F	U	$T_{\text{adv}} = \frac{R}{U}$	$T_{\text{diff}} = \frac{R^2}{D}$	$\text{Pe} = \frac{T_{\text{diff}}}{T_{\text{adv}}}$
	100	50	$\sim \eta U \delta$	100	1	10	10
(units)	(μm)	(μm)	(pN)	($\mu\text{m}\cdot\text{s}^{-1}$)	(s)	(s)	–
Dimensionless	$\tilde{R} = \frac{R}{R}$	$\tilde{h} = \frac{h}{R}$	$\tilde{F}$	$\tilde{U}$	$\frac{\tilde{R}}{\tilde{U}}$	$\frac{\tilde{R}}{\tilde{U}}\text{Pe}$	Pe
	1	0.5	5	≈ 1	1	10	10

proposed in [13]. Here, we limit our analysis to forces that are radially directed towards the center of the sphere, although the method can account for forces of arbitrary directions.

Calibrating the dimensionless strength and regularization parameter of the regularized Stokeslet. According to our experimental observations, a single ciliate of height $h \approx 50\mu$m attached to a diatom of size $R \approx 100\mu$m produces a dimensional flow with maximal flow speeds in the range of $U \approx 100$–$500\mu\text{m} \cdot \text{s}^{-1}$.

We calibrate the dimensionless strength $\tilde{F}$ of the Stokeslet to produce dimensionless flows, that when re-scaled to dimensional units, have similar values as those observed experimentally. We find that, when a single dimensionless Stokeslet is regularized over a region of size $\tilde{\delta} = \delta/R$, where δ is the radius of the ciliated crown, and placed at a relative distance $\tilde{h} = h/R$ from the sphere's surface, the maximum speed generated by the Stokeslet is about $\tilde{U} = 1$ when the Stokeslet strength is set to $\tilde{F} = 5$. Whereas for the same geometric parameters, a Stokeslet of strength $\tilde{F} = 25$ produces a flow field where the maximum speed $\tilde{U}$ is 5 fold larger.

In dimensional units, using the advective time scale $T_{\text{adv}} = 1$ s and $R = 100$ μm leads to a characteristic flow speed $U = \tilde{U}R/T_{\text{adv}} = 100$ $\mu\text{m} \cdot \text{s}^{-1}$ for the regularized Stokeslet of strength $\tilde{F} = 5$, whereas for the

advective time scale $T_{\text{adv}} = 0.2$ s, we get the characteristic flow speed is $U = 500\mu\text{m} \cdot \text{s}^{-1}$ for $\tilde{F} = 25$; see Table S2.

Choice of force locations. Ciliates typically attach randomly on either or both sides of the diatom. However, statistics of the attachment sites are currently lacking. In the absence of empirical guidelines of the ciliate attachment sites, we need to make assumptions in order to proceed with our modeling efforts. Here, we make two main assumptions as follows.

1. We assume that the ciliates are attached symmetrically on both sides of the diatom such that the total forces and total moments acting on the diatom due to the ciliates are balanced. The diatom-ciliate system is thus stationary. This assumption allows us to isolate the effect of ciliate-driven flows on nutrient uptake in the absence of net rotations or translations of the diatom-ciliate system. Net motions serve to enhance nutrient uptake in various microscopic systems [9, 14]. Therefore, we expect this stationarity assumption to provide a lower bound on the potential enhancement in nutrient uptake to the diatom.

2. We assume that on each side of the diatom, the ciliates are attached following a pattern that results in zero net azimuthal velocity. This assumption is convenient because it allows us to make progress in evaluating the an effective average behavior of the ambient concentration field based on the axisymmetric formulation of the advection-diffusion equation in (7). Axisymmetry is typically destroyed when multiple Stokeslet forces are present in random locations and even at regular attachment sites as detailed in Table S3. In fact, regularity is not essential here and it is only useful for us in as far as it guarantees zero net azimuthal velocity, i.e., zero net velocity in the ϕ direction. In such case, we can average the fluid velocity in the ϕ direction and obtain an average velocity field in the fluid domain around the diatom. Specifically, starting from either random or regular attachment sites that result in zero net velocity in the ϕ direction, we first compute the three-dimensional fluid velocity $\mathbf{u}(r, \theta, \phi) \equiv (u_r, u_\theta, u_\phi)$ according to [13], then we calculate the average velocity $(1/2\pi) \int_0^{2\pi} \mathbf{u}(r, \theta, \phi) d\phi$, which due to the choice of Stokeslet distribution has zero averaged ϕ-component. We arrive at a two-dimensional average velocity field $\langle \mathbf{u} \rangle \equiv (u_r(r, \theta), u_\theta(r, \theta))$, which encodes the averaged effect of the distribution of Stokeslets. We use this velocity to numerically solve the axisymmetric advection-diffusion equation (7) as detailed above.

We emphasize that these choices are made for convenience, in order to obtain conservative estimates of the range of potential improvement in the diatom nutrient uptake due to ciliate-driven flows. Diatom-ciliate consortia do not follow a symmetric distribution of ciliates, and imbalance in forces due to the ciliates cause the diatom to translate and rotate as depicted in Movie S5. These motions are known to enhance nutrient uptake [9, 14] and they are not included in our conservative estimates of the enhancement in the Sherwood number.

Sherwood Number

Definition of Sherwood number. By definition, the Sherwood number is given by the ratio of advective plus diffusive nutrient flux normalized by the diffusive nutrient flux, which in the spherical model considered here amounts to

$$\text{Sh} = \frac{I}{I_{\text{diffusion}}} = \frac{\oint D\mathbf{n} \cdot \nabla C dS}{4\pi D C_\infty R} = \frac{\oint D(\partial C/\partial r)(2\pi R^2 \sin\theta) \text{d}\theta}{4\pi D C_\infty R} = \frac{1}{2} \oint \frac{\partial (C/C_\infty)}{\partial (r/R)} (\sin\theta) \text{d}\theta. \tag{10}$$

Sinking diatom. We use the relationship between Sh and Pe that was suggested by [15] and employed in [2],

$$\text{Sh} = \frac{1}{2}(1 + (1 + 2\text{Pe})^{1/3}). \tag{11}$$

The relationship in (11) is valid for all Pe around uniformly translating spheres in Stokes flows. In the region $0.0015 < \text{Pe} < 0.1$, it agrees within 0.7% of the analytic limit at small Pe of Acrivos & Taylor (1962) [8], and

Table S3: **Computational results:** in all computations, we consider a pair of diametrically-opposite identical Stokeslets of equal strength $\tilde{F}$ that is set to $\tilde{F} = 5$ or $\tilde{F} = 25$ as discussed in table S2. The radius of diatom R is varied while the dimensions of the ciliate are considered fixed; see Fig. S5 and TableS7. The regularization parameter is set to the dimensionless radius of the ciliated crown δ/R where $\delta \approx h/2$ and $h \approx 50$ μm consistent with Table S7. When solving the dimensionless advection-diffusion equation (6), the value of Péclet number is set to Pe = 10 for $\tilde{F} = 5$ and Pe= 100 for $\tilde{F} = 25$.

Case	R (μm)	h (μm)	δ (μm)	h/R	δ/R	$\tilde{F}$	Pe	N	Sh
1a	50	50	25	1	1/2	5	10	2	1.1752
1b	50	50	25	1	1/2	25	100	2	3.7919
2a	100	50	25	1/2	1/4	5	10	2	1.1317
2b	100	50	25	1/2	1/4	25	100	2	3.8851
3a	150	50	25	1/3	1/6	5	10	2	1.1103
3b	150	50	25	1/3	1/6	25	100	2	3.6668
4a	200	50	25	1/4	1/8	5	10	2	1.1006
4b	200	50	25	1/4	1/8	25	100	2	3.3871
5a	250	50	25	1/5	1/10	5	10	2	1.0957
5b	250	50	25	1/5	1/10	25	100	2	3.0919

in the region $100 < \text{Pe} < 5000$, it agrees within 2% of the analytic limit at large Pe of Acrivos & Goddard (1965) [16]; see [2] for more details.

We calculate the Péclet number for sinking diatoms using $\text{Pe} = UR/D$, where U is given by (1). We consider diatoms up to $R = 250$ μm in radius (that is, 500 μm in diameter) sinking at $\Delta\rho = 10$ kg·m^{-3} and $\Delta\rho = 100$ kg·m^{-3} and $D = 10^{-9}$ m^2·s^{-1}, as shown in Fig. S2.

Diatom-ciliate system. Eq. (11) is valid for uniformly translating spheres only. In fact, instead of (11), we can calculate the Sherwood number directly from the numerical solution of the concentration field based on (10), as done in the data points shown in Fig. S2. We use this direct approach in the diatom-ciliate analysis.

Parametric study

It is instructive to list all parameters in dimensional form and build non-dimensional counterparts using Buckingham theorem.

Sinking diatom. We have seven dimensional parameters: the acceleration due to gravity g, fluid viscosity η, fluid density ρ, diatom density relative to the fluid $\Delta\rho$, diatom radius R, sinking velocity U, and nutrient diffusivity D, that can be grouped into four non-dimensional parameters: the density ratio $\Delta\rho/\rho$, Péclet number $\text{Pe} = UR/D$, drag-to-weight ratio $F_{\text{drag}}/W = \eta U/g\Delta\rho R^2$, and Schmidt number $\text{Sc}=\rho D/\eta$. Considering a particular fluid medium ρ and η and nutrient diffusivity D, the diatom can modulate its density $\Delta\rho$, and its size R can vary. As these two quantities vary, they determine the sinking speed U and in turn the Péclet number $\text{Pe} = UR/D$. For our analysis, we use the upper limit of $\Delta\rho$ and consider one free parameter: the diatom radius R, which determines Pe and consequently Sh.

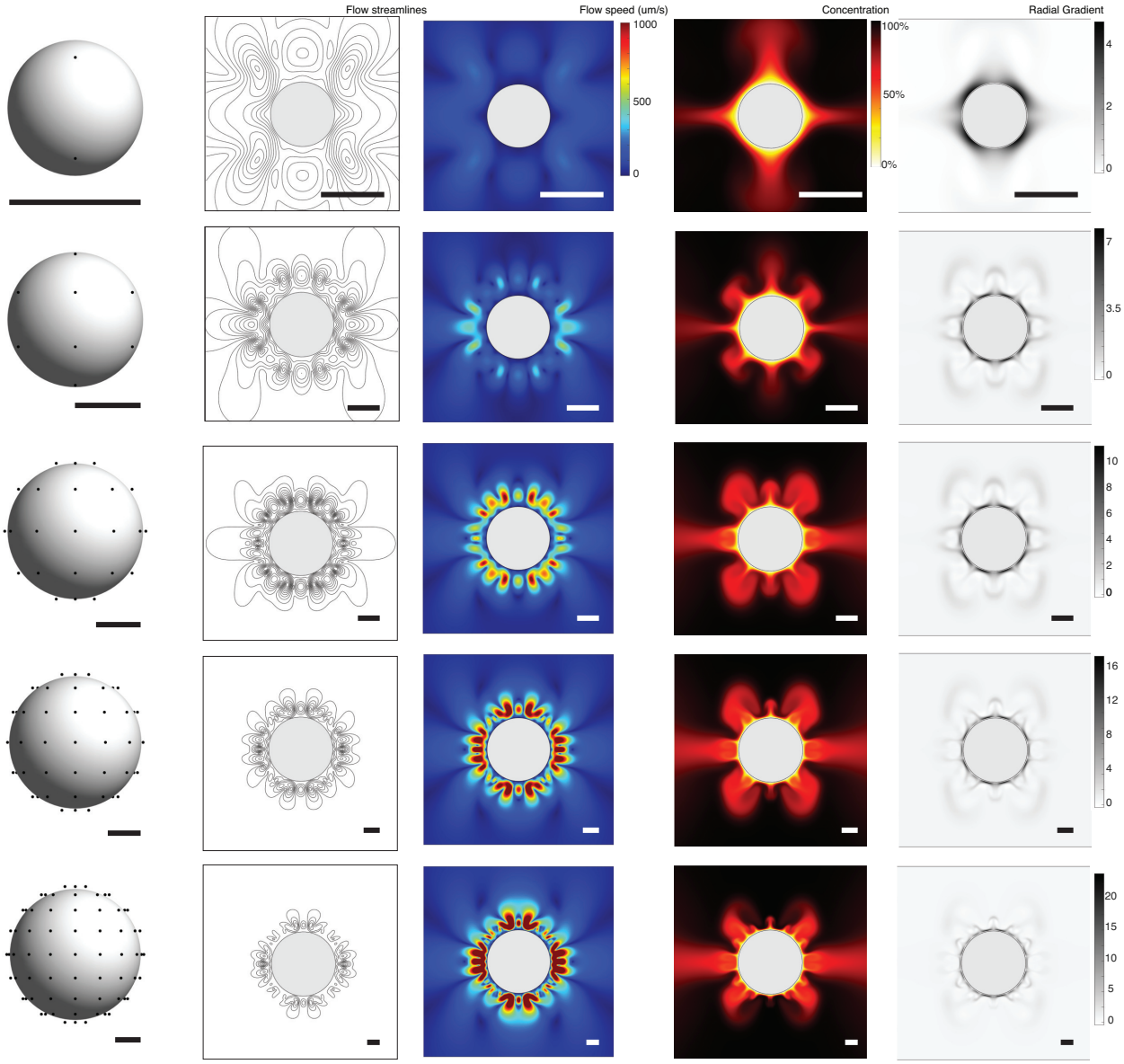

Figure S4: **Ciliate-diatom system:** Parameter values from top to bottom are listed in Table S4. Scale bars represent 100 microns in length. Note that sphere diameter increases from top to bottom reflecting the potential for more ciliates on larger diatoms. (left) ciliate location, (middle left) contours of constant flow speed (middle) ϕ-averaged flow speed, (middle right) concentration field, (right) radial concentration gradient.

Diatom-ciliate system. We have eight dimensional parameters: the fluid viscosity η, fluid density ρ, diatom radius R, ciliate-induced fluid velocity U, ciliate force F, ciliate height h, ciliate radius δ, and nutrient diffusivity D. We can group them into five non-dimensional parameters: Sc=$\rho D/\eta$, Pe = UR/D, $F/(\eta U\delta)$, h/R and δ/R. For a known fluid medium ρ and η and nutrient diffusivity D, the size R of the diatom can vary. We consider two limits of dimensionless ciliate force strength: $\tilde{F} = 5$ and $\tilde{F} = 25$ which produce maximal flow speeds equal to $\tilde{U} \approx 1$ and $\tilde{U} \approx 5$ and correspondingly, $U = 100\mu\text{m} \cdot \text{s}^{-1}$ and $U = 500$ $\mu\text{m} \cdot \text{s}^{-1}$ in dimensional units, when located outside a sphere of radius $R = 100$ μm (see tables S2 and S3). We assume no variation in the height h and radius δ of the ciliate.

Table S4: **Multiple ciliates:** in all computations, the dimensionless value of the Stokeslet force is set to $\tilde{F} = 25$ when solving the dimensionless Stokes equations (2). The value of Péclet number is set to Pe= 100 when solving the dimensionless advection-diffusion equation (6).

Case	(1)	(2)	(3)	(4)	(5)
Diatom radius R (μm)	50	100	150	200	250
Ciliate radius δ (μm)	25	25	25	25	25
Number of ciliates $N = \dfrac{4\pi R^2}{\pi(2\delta)^2}$	4	16	36	64	100
Sherwood number Sh	3.6695	5.4673	7.1780	8.7936	10.1550

Maximum number of attached ciliates. The maximum number of attached ciliates can be estimated by dividing the total surface area of the diatom by the area of the ciliated crown; specifically, $4\pi(R+h)^2/\pi\delta^2$ is the number of ciliates that provides complete covering the spherical surface of radius $R+h$ at the location of the ciliate crown. Here, to obtain a rough estimate of the maximum number of attached ciliates that does not completely cover the sphere, we assume an exclusion zone of area $\pi(2\delta)^2$ around the center of each ciliate. We arrive at the number of ciliates N listed in table S4 as a function of the diatom radius.

Uniform covering of the diatom surface via equal-area partition. We partition the surface of the sphere into N equal-area parts and locate the ciliate (Stokeslet) at the center of each partition. This guarantees that the Stokeslets uniformly cover the surface of the sphere. We use a common algorithm for the equal-area partition based on the Rakhmanov-Saff-Zhou procedure; see e.g. [17]. Starting from the equal area requirement, the length scale of each partition is the square-root of the partition area. We then construct the latitude and longitude of each partition and the corresponding mid-point.

Experimental measurements of diatom sinking rates

We compiled a set of experimental data on *Coscinodiscus* sinking rates for comparison with epibiont flows. Sinking rates in the literature are highly variable and believed to be related to the nutrient status of cells [18, 19]. Lower internal nutrient levels are thought to be related to higher sinking rates. Additionally, the method of sinking rate determination influences published rates. Most published rates were average rates recorded over hour-long time scales. However, Gemmell *et al.* found that rates varied on much shorter time scales – often minutes – and that longer average values underestimated more rapid short-term rates [6]. Nutrients alone do not explain all patterns because rates are much lower in the dark. Du Close *et al.* argue that this is because regulation of sinking rate, particularly rapid sinking, is metabolically expensive for the cell and photosynthesis is required to attain the highest rates [20].

We can thus conclude that variable rates reflect a variety of cell physiological states. For our purpose of comparing nutrient enhancement mechanisms for a phytoplankton cell, the highest sinking rates represent the most pronounced cases of potential nutrient enhancement. Lower sinking rates of healthy and dividing cells do not represent the state at which nutrient enhancement is maximized by sinking. For brief periods, diatoms can even show positive buoyancy. In contrast, high sinking rates represent the most conservative comparison because they demonstrate the highest potential of sinking for nutrient enhancement. Following this logic, we include the highest sinking rates for studies that also include cell diameter information (Table S5). Cell diameter data was not listed for some studies. In one study, the average cell diameter (43 microns) was far below any other reports for *Coscinodiscus wailesii* [18]. Table S5 represents these extremes in sinking rate and associated diameters, as well as our calculation of the associated $\mathrm{Pe} = UR/D$ using $D = 10^{-9}\ \mathrm{m}^2 \cdot \mathrm{s}^{-1}$ and Sh based on (11).

Table S5: **Experimental measurements** of sinking rates of *Coscinodiscus wailesii*. Péclet based on $D = 10^{-9}\mathrm{m}^2 \cdot \mathrm{s}^{-1}$. Sherwood number is calculated based on Eq. (11).

Source	R (μm)	U ($\mu\mathrm{m} \cdot \mathrm{s}^{-1}$)	Pe	Sh
Bianfeng 1982 [18]	16	45	0.72	1.17
Smayda 1970 [21]	70	81–350	5.67–24.50	1.65 – 2.34
Gemmell *et al.* 2016 [6]	122.5	10–770	1.225 –94.325	1.25–3.37
Du Clos *et al.* 2019 [20]	150	180–520	27–78	2.40–3.20
Ono *et al.* 2006 [22]	–	9–48	–	–
Miklasz & Denny 2010 [1]	84–132	6–407	0.50–54.0	1.13–2.89

Table S6: **Comparative volume-specific clearance rates of planktonic protists.** Rates were based on particle removal except for $*$, which were based on direct optical measurement of flows.

Source	Protist studied	Specific clearance rate (body volume $\cdot\mathrm{hr}^{-1}$)
Fenchel 1982	4 marine, 2 freshwater species of pelagic flagellates	5.2 $\times 10^4$- 1.1 $\times 10^6$
Boenigk & Arndt 2000$*$	1 marine, 3 freshwater species of pelagic flagellates	0.8 $\times 10^5$- 3.3 $\times 10^5$
Sherr & Sherr 1987	9 species of marine pelagic ciliates	4.0 $\times 10^4$ - 6.8 $\times 10^5$
Hadas et al. 1998	3 species of freshwater pelagic ciliates	9.7 $\times 10^3$ - 1.5 $\times 10^6$
Stabell 1996	2 species of freshwater pelagic ciliates	9.7 $\times 10^3$ - 1.5 $\times 10^6$
Zimmermann-Timm & Barkmann 2000	2 species of freshwater pelagic ciliates	1.4 $\times 10^5$- 8.7 $\times 10^5$
Simek et al 1995	12 species of freshwater pelagic ciliates	0.5 $\times 10^4$- 4.2 $\times 10^5$
Present study$*$	*Pseudovorticella coscinodisci*	1.8 $\times 10^5$- 3.8 $\times 10^5$

Experimental measurements of protist flow rates

Flow fields of replicate (n=8) *P. coscinodisci* ciliates were measured to determine fluid flux rates. Flow speeds were collected for each PIV interrogation window along transects through ciliate flow fields (Fig. 1C from main body duplicated below). That transect served as the diameter of a circle describing the ciliate flow field 3D dimensions. As noted in the main text, we distinguished between flux due to flow through the ciliary crown area (flow directly entering the ciliary crown represents flows from which the ciliate could clear prey, Fig 1A magenta portion of transect) and non-crown area (flows outside the ciliary crown and therefore not entering the crown region or available for ciliate feeding, Fig 1A blue portion of transect) for each replicate ciliate. These values were compared to literature values by expressing flux rates in terms of body volume (average body volume of $1.95 \times 10^4 \mathrm{microns}^3$, Table S5) to arrive at the range of body volume specific fluid flux rates per ciliate. The volume-specific flux rates we list represent, at a low level, solely the average crown flux ($1.8 \times 10^5 \mathrm{ciliate}^{-1}\mathrm{hr}^{-1}$) and at a higher level, the summed crown and non-crown flux ($3.8 \times 10^5 \mathrm{ciliate}^{-1}\mathrm{hr}^{-1}$) noted in the text and in Table S4. We delineate these two types of flux rate for comparison to literature values because, while total flux rate is important for transport of dissolved nutrients to the diatom, many protistan volume-specific flux rates are calculated based on removal of prey from the fluid (Table S4), which requires passage through the ciliate crown and are better compared to our lower,

crown-only volume-specific flux rate.

We compiled a set of experimental data on protist flow rates for comparison with epibiont flows observed in our study. Results are shown in Table S6.

Supporting Information Movies

Movie S1. Streak flows around *Coscinodiscus wailesii* diatom host with multiple attached *Pseudovorticella coscinodisci* ciliate epibionts. Diatom cell diameter is 295 μm. Original images were captured at 125 fps, streak lines were derived integrating particle paths over 500 frame intervals and played back at 10 fps.

Movie S2. Flows around *Coscinodiscus wailesii* diatom host with an attached *Pseudovorticella coscinodisci* ciliate epibiont. The ciliate feeding current draws fluid towards the ciliated crown, past the ciliate and along the diatom cell body. Substantially more fluid is transported by the ciliary incurrent than is passed through the ciliary sorting surfaces and ejected as a processed feeding excurrent (to the right in the image). Original image captured at 1000 fps, played back at 100 fps. Diatom cell diameter is 295 μm; ciliate crown width is 49 m. Particles are a whole milk suspension (5% by volume). This image was re-oriented for measurements made in Fig. 1B,C.

Movie S3. Flow streak lines around *Coscinodiscus wailesii* diatom host with an attached *Pseudovorticella coscinodisci* ciliate epibiont. Streak lines were derived from the image sequence of Movie 2 by integrating particle paths over 200 frame intervals.

Movie S4. Flow generated by multiple *Pseudovorticella coscinodisci* ciliate epibionts on a 350 μm diameter *Coscinodiscus wailesii* diatom host with playback at real time. Images captured and played at 125 fps. The distinct plumes are formed by the excurrents of nine individual ciliate epibionts on the surface away from the camera lens.

Movie S5. Rotation of *Coscinodiscus wailesii* diatom host with multiple attached *Pseudovorticella coscinodisci* ciliate epibionts. Unbalanced forces generated by ciliates result in rotational motion of consortia.

Quantification of protistan physical dimensions

Measurements of protistan crown area and body volumes utilized images (Fig. S5) of individuals (Table S5).

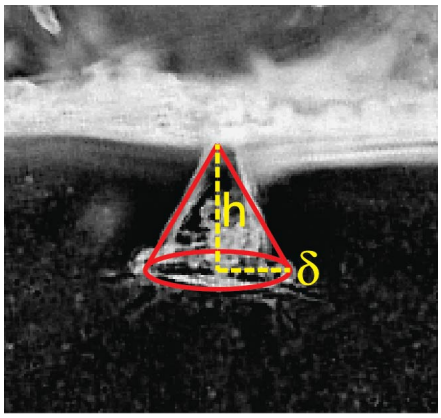

Figure S5: Depiction of the method used to estimate physical dimensions of *Pseudovorticella coscinodisci* epibionts. Cell height and ciliary crown radius were combined to approximate the volume of a ciliate as a conical form.

Table S7: **Morphological dimensions of *Pseudovorticella coscinodisci*** (n = 56).

Height (microns)	**Width** (microns)	**Volume** (microns^3)	**Height** (microns)	**Width** (microns)	**Volume** (microns^3)
42.9	45.1	22917.6	49.9	39.1	19975.9
41.8	40.3	17750.6	46.2	41.4	20772.3
41.0	50.0	26857.2	41.9	35.8	14090.0
46.4	43.1	22540.6	36.6	36.7	12876.2
54.3	49.0	34190.4	55.6	40.3	23626.6
43.9	32.3	11959.9	44.3	41.9	20342.9
40.8	44.0	20701.3	44.2	34.7	13936.1
38.9	33.7	11572.0	52.4	38.7	20556.6
41.3	42.0	19098.5	46.3	38.9	18293.2
44.8	39.2	17985.5	37.4	35.6	12428.0
68.5	50.0	44845.4	49.6	47.0	28693.4
56.5	31.6	14721.9	46.3	41.6	21004.9
39.4	36.4	13642.0	46.9	39.9	19557.4
39.7	39.8	16409.9	47.6	44.6	24824.6
56.5	49.8	36635.6	43.4	41.5	19538.9
48.5	40.9	21275.4	33.1	39.0	13191.0
38.2	36.8	13560.0	43.9	47.2	25674.9
41.0	38.0	15482.1	38.9	34.7	12250.9
47.2	45.4	25437.6	36.4	43.2	17782.9
43.1	44.8	22589.2	38.7	38.0	14631.7
48.3	47.2	28175.1	50.1	41.0	22042.5
41.4	40.9	18144.2	46.8	41.5	21112.3
40.7	32.6	11302.0	39.6	40.9	17375.9
41.9	33.7	12474.4	44.0	49.7	28490.9
37.7	35.9	12766.7	46.0	43.0	22280.1
35.8	37.3	13055.9	48.7	44.9	25632.8
38.9	32.5	10777.7	43.9	37.8	16385.5
37.7	35.3	12305.8	42.1	39.1	16833.1

	Height (microns)	**Width** (microns)	**Volume** (microns^3)
Average	44.2	40.5	19524.6
Standard Deviation	6.2	4.9	6786.4

References

[1] Miklasz KA, Denny MW. Diatom sinkings speeds: Improved predictions and insight from a modified Stokes' law. Limnology and Oceanography. 2010;55(6):2513–2525. Available from: https://aslopubs.onlinelibrary.wiley.com/doi/abs/10.4319/lo.2010.55.6.2513.

[2] Karp-Boss L, Boss E, Jumars P, et al. Nutrient fluxes to planktonic osmotrophs in the presence of fluid motion. Oceanography and Marine Biology. 1996;34:71–108.

[3] Berg HC, Purcell EM. Physics of chemoreception. Biophysical Journal. 1977 2020/01/24;20(2):193–219. Available from: https://doi.org/10.1016/S0006-3495(77)85544-6.

[4] Short MB, Solari CA, Ganguly S, Powers TR, Kessler JO, Goldstein RE. Flows driven by flagella of multicellular organisms enhance long-range molecular transport. Proceedings of the National Academy

of Sciences. 2006;103(22):8315–8319. Available from: https://www.pnas.org/content/103/22/8315.

[5] Kiørboe T, Ploug H, Thygesen UH. Fluid motion and solute distribution around sinking aggregates. I. Small-scale fluxes and heterogeneity of nutrients in the pelagic environment. Marine Ecology Progress Series. 2001;211:1–13.

[6] Gemmell BJ, Oh G, Buskey EJ, Villareal TA. Dynamic sinking behaviour in marine phytoplankton: rapid changes in buoyancy may aid in nutrient uptake. Proceedings of the Royal Society B. 2016;283:20161126.

[7] Happel J, Brenner H. Low Reynolds number hydrodynamics: with special applications to particulate media. vol. 1. Springer Science & Business Media; 2012.

[8] Acrivos A, Taylor TD. Heat and Mass Transfer from Single Spheres in Stokes Flow. The Physics of Fluids. 1962;5(4):387–394. Available from: https://aip.scitation.org/doi/abs/10.1063/1.1706630.

[9] Michelin S, Lauga E. Optimal feeding is optimal swimming for all Péclet numbers. Physics of Fluids. 2011;23(10):101901. Available from: https://doi.org/10.1063/1.3642645.

[10] Pepper RE, Roper M, Ryu S, Matsudaira P, Stone HA. Nearby boundaries create eddies near microscopic filter feeders. Journal of the Royal Society Interface. 2010;7(46):851–862.

[11] Pepper RE, Roper M, Ryu S, Matsumoto N, Nagai M, Stone HA. A new angle on microscopic suspension feeders near boundaries. Biophysical journal. 2013;105(8):1796–1804.

[12] Kim S, Karrila SJ. Microhydrodynamics: principles and selected applications. Courier Corporation; 2013.

[13] Wróbel JK, Cortez R, Varela D, Fauci L. Regularized image system for Stokes flow outside a solid sphere. Journal of Computational Physics. 2016;317:165–184.

[14] Andersen A, Kiørboe T. The effect of tethering on the clearance rate of suspension-feeding plankton. Proceedings of the National Academy of Sciences. 2020;117(48):30101–30103. Available from: https://www.pnas.org/content/117/48/30101.

[15] Clift R, Grace JR, Weber ME. Bubbles, drops, and particles. Courier Corporation; 1978.

[16] Acrivos A, Goddard JD. Asymptotic expansions for laminar forced-convection heat and mass transfer. Journal of Fluid Mechanics. 1965;23(2):273?291.

[17] Saff EB, Kuijlaars ABJ. Distributing many points on a sphere. The Mathematical Intelligencer. 1997;19(1):5–11. Available from: https://doi.org/10.1007/BF03024331.

[18] Bienfang P, Harrison P, Quarmby L. Sinking rate response to depletion of nitrate, phosphate and silicate in four marine diatoms. Marine Biology. 1982;67(3):295–302.

[19] Mann K, Lazier J. Vertical Structure of the Open Ocean: Biology of the Mixed Layer. Dynamics of Marine Ecosystems. Oxford: Blackwell Publishing; 2006.

[20] Du Clos K, Karp-Boss L, Villareal T, Gemmell B. Coscinodiscus wailesii mutes unsteady sinking in dark conditions. Biology letters. 2019;15(3):20180816.

[21] Smayda TJ. Normal and accelerated sinking of phytoplankton in the sea. Marine Geology. 1971;11(2):105–122.

[22] Ono A, Ichimi K, Tada K. The standing stock and sinking rate of the large diatom Coscinodiscus wailesii causing Nori (Porphyra) discoloration. Bull Soc Sea Water Sci Jpn. 2006;60:253–259.